

Supporting Information for

**Macrocycle supported dimetallic lanthanide complexes
with slow magnetic relaxation in Dy₂ analogues**

Fu-Xing Shen,^{a,1} Kuheli Pramanik,^{b,c,1} Paula Brandão,^d Yi-Quan Zhang,^e Narayan Ch.

Jana,^b Xin-Yi Wang,^a Anangamohan Panja^{b,c}

^a State Key Laboratory of Coordination Chemistry, Collaborative Innovation Center of Advanced Microstructures, School of Chemistry and Chemical Engineering, Nanjing University, Nanjing, 210023, China. E-mail: wangxy66@nju.edu.cn

^b Department of Chemistry, Panskura Banamali College, Panskura RS, WB 721152, India. E-mail: ampanja@yahoo.co.in

^c Department of Chemistry, Gokhale Memorial Girls' College, 1/1 Harish Mukherjee Road, Kolkata 700020, India

^d Department of Chemistry, CICECO-Aveiro Institute of Materials, University of Aveiro, 3810

^e Jiangsu Key Laboratory for NSLSCS, School of Physical Science and Technology, Nanjing Normal University, Nanjing 210023, China

¹ These authors contributed equally to this work.

Table of Content

Fig. S1. ^1H NMR spectrum of the Schiff base ligand HL in CDCl_3	4
Fig. S2. Experimental and simulated powder X-ray diffraction patterns for $\mathbf{1}_{\text{Dy}}\text{-}\mathbf{6}_{\text{Gd}}$. The data were collected at room temperature. The good fit of the experimental and simulated patterns indicates the phase purity of these compounds.....	5
Fig. S3. Electrospray ionization mass spectrum (ESI-MS positive) of the Schiff base ligand in methanol (top) and its expanded view at bottom.....	6
Fig. S4. Electrospray ionization mass spectra (ESI-MS positive) of a reaction mixture recorded after 5 min (top) and 1 h (bottom) of mixing.....	7
Scheme S1. Probable mechanism for the <i>in-situ</i> transformation of the Schiff base leading to the macrocyclic ligand.....	8
Fig. S5. Crystal packing of complexes $\mathbf{1}_{\text{Dy}}$ and $\mathbf{4}_{\text{Dy}}$ along the a axis. The numbers show the shortest Dy-Dy distances between the adjacent Dy_2 units.....	9
Fig. S6. The plot of $1/\chi_M$ versus T for $\mathbf{3}_{\text{Gd}}$ (a) and $\mathbf{6}_{\text{Gd}}$ (b), and the linear fit of Curie-Weiss law. The solid lines represent the best fits according to the Curie-Weiss law.....	9
Fig. S7. Field dependent magnetization curves for compounds $\mathbf{1}_{\text{Dy}}$, $\mathbf{2}_{\text{Tb}}$, $\mathbf{4}_{\text{Dy}}$ and $\mathbf{5}_{\text{Tb}}$ at 2.0 K.....	10
Fig. S8. Frequency dependent in-phase (χ') and out-of phase (χ'') signals of the ac susceptibility for $\mathbf{2}_{\text{Tb}}$ under applied $H_{\text{dc}} = 0$ and 1 kOe.....	10
Fig. S9. Frequency dependent in-phase (χ') and out-of phase (χ'') signals of the ac susceptibility for $\mathbf{5}_{\text{Tb}}$ under applied $H_{\text{dc}} = 0$ and 1 kOe.....	11
Fig. S10. Temperature dependent in-phase (χ') and out-of phase (χ'') signals of the ac susceptibility for $\mathbf{1}_{\text{Dy}}$ and $\mathbf{4}_{\text{Dy}}$ under zero dc field.....	11
Electrostatic model for $\mathbf{1}_{\text{Dy}}$ and $\mathbf{4}_{\text{Dy}}$	12
Fig. S11. Partial charges assigned to the formally charged ligands in complexes $\mathbf{1}_{\text{Dy}}$ and $\mathbf{4}_{\text{Dy}}$	12
Fig. S12. Ground state magnetic anisotropy of complexes $\mathbf{1}_{\text{Dy}}$ (a) and $\mathbf{4}_{\text{Dy}}$ (b). The Green rods represent the orientations of the electrostatic anisotropy axes for each of the two Dy^{III} ions in complexes $\mathbf{1}_{\text{Dy}}$ and $\mathbf{4}_{\text{Dy}}$ as calculated by electrostatic model.....	13
Table S1. Selected bond lengths (\AA) for complex $\mathbf{1}_{\text{Dy}}\text{-}\mathbf{6}_{\text{Gd}}$	13
Table S2. SHAPE analysis of the Ln^{III} ion in complexes $\mathbf{1}_{\text{Dy}}\text{-}\mathbf{6}_{\text{Gd}}$	14
Table S3. Relaxation fitting parameters from the least-square fitting of the Cole-Cole plots of $\mathbf{1}_{\text{Dy}}$ under 2.0 K-7.0 K according to the generalized Debye model.....	14
Table S4. Relaxation fitting parameters from the least-square fitting of the Cole-Cole plots of $\mathbf{4}_{\text{Dy}}$ under 2.0 K-10.0 K according to the generalized Debye model.....	15
Table S5. Parameters fitted from the Arrhenius plots considering multiple relaxation processes for $\mathbf{1}_{\text{Dy}}$ and $\mathbf{4}_{\text{Dy}}$	15

Computational details	16
Fig. S13. Calculated complete structures of complexes 1_{Dy} and 4_{Dy} ; H atoms are omitted.....	16
Table S6. Calculated energy levels (cm ⁻¹), g (g_x , g_y , g_z) tensors and predominant m_J values of the lowest eight Kramers doublets (KDs) of individual Dy ^{III} fragments for complexes 1_{Dy} and 4_{Dy} using CASSCF/RASSI-SO with MOLCAS 8.4.....	17
Table S7. Wave functions with definite projection of the total moment m_J > for the lowest two KDs of individual Dy ^{III} fragments for complexes 1_{Dy} and 4_{Dy}	18
Table S8. Exchange energies E (cm ⁻¹), the energy difference between each exchange doublets Δ_t (cm ⁻¹) and the main values of the g_z for the lowest two exchange doublets of 1_{Dy} and 4_{Dy}	19
Reference	19

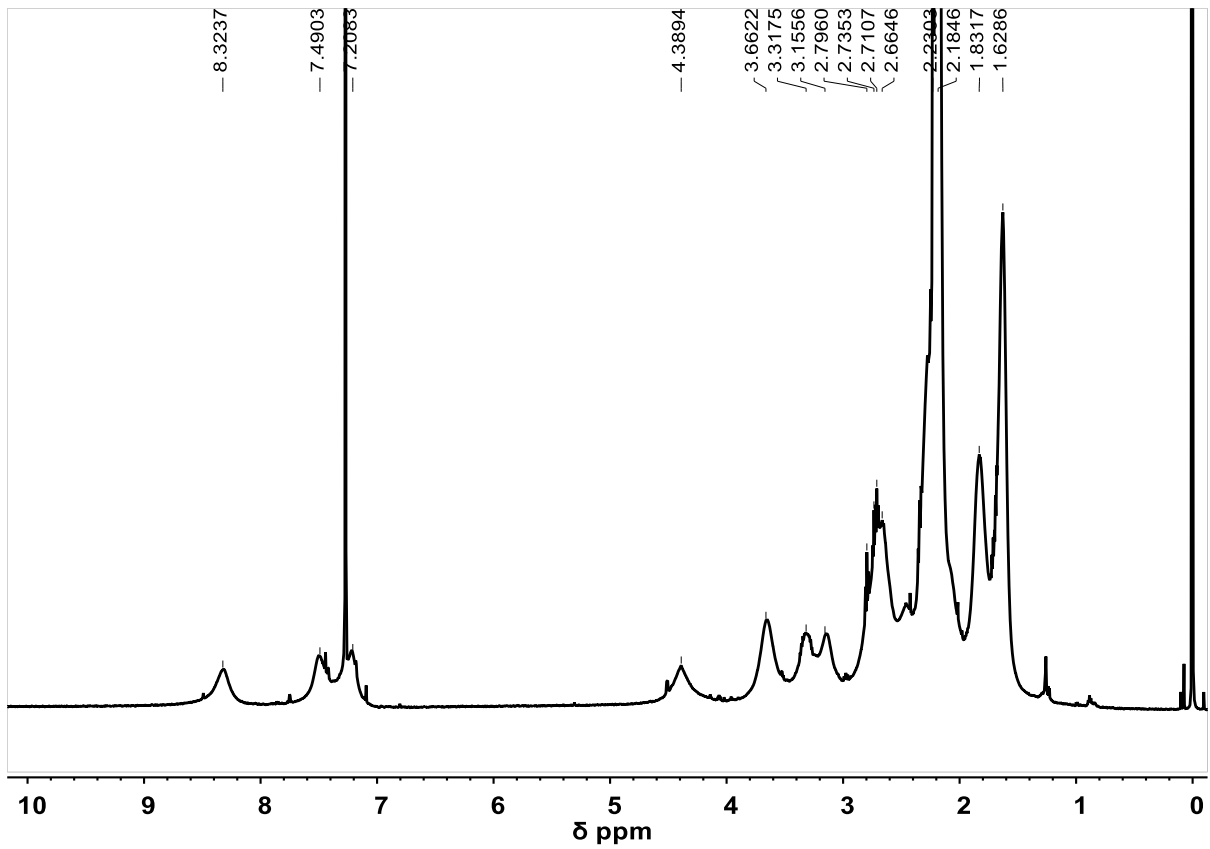


Fig. S1. ^1H NMR spectrum of the Schiff base ligand HL in CDCl_3 .

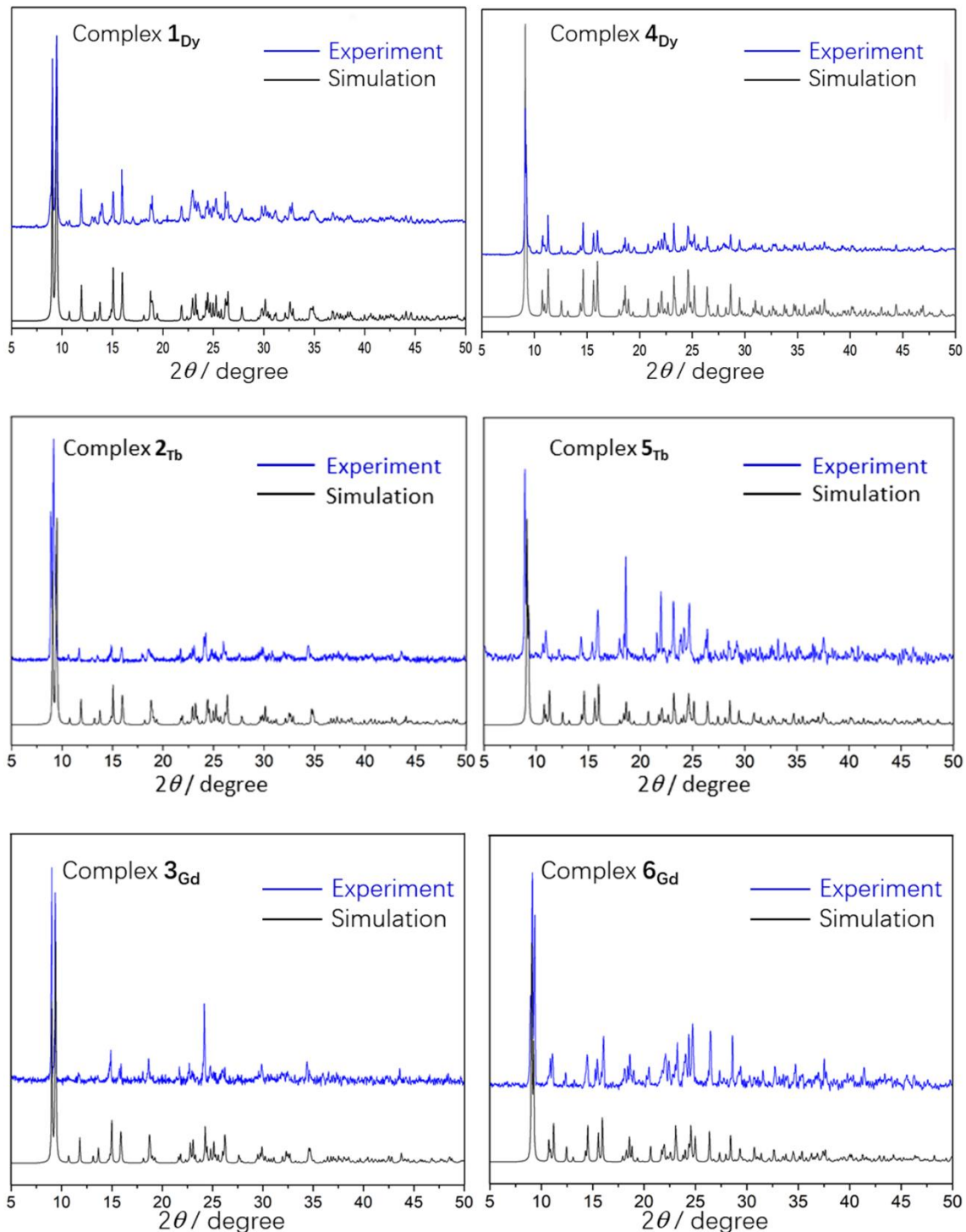


Fig. S2. Experimental and simulated powder X-ray diffraction patterns for **1_{Dy}-6_{Gd}**. The data were collected at room temperature. The good fit of the experimental and simulated patterns indicates the phase purity of these compounds.

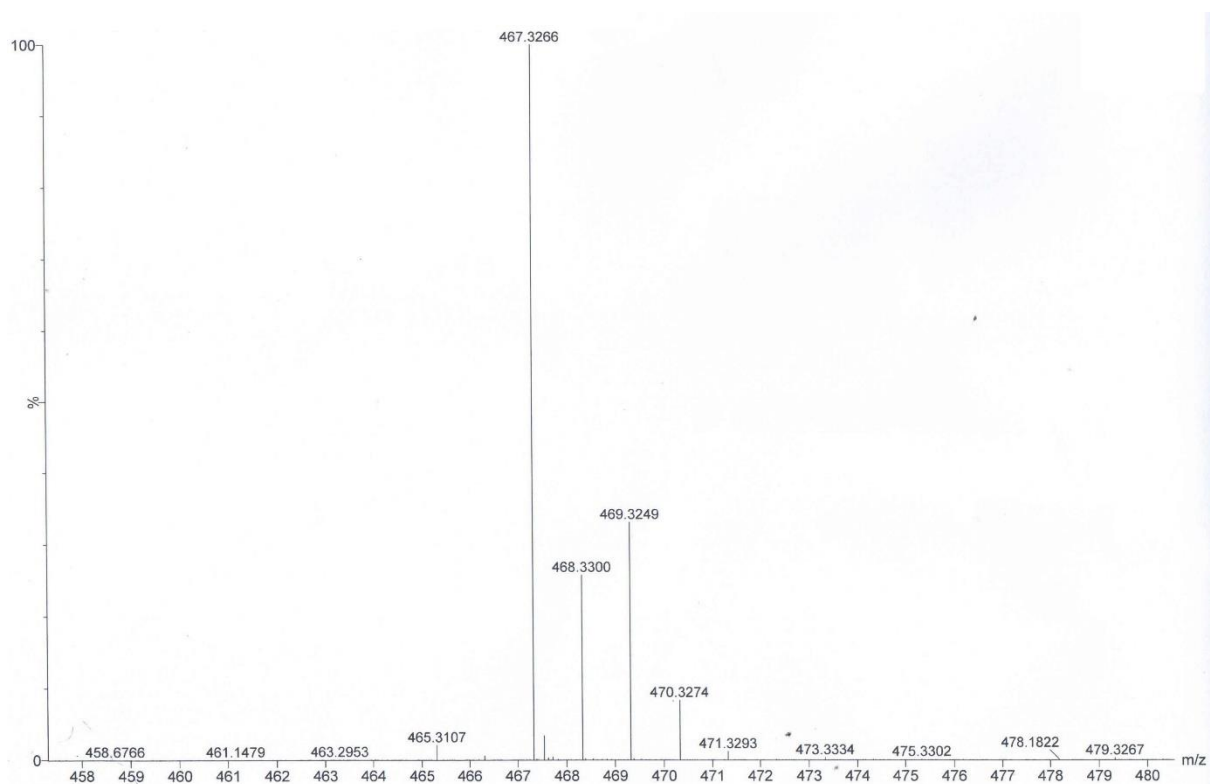
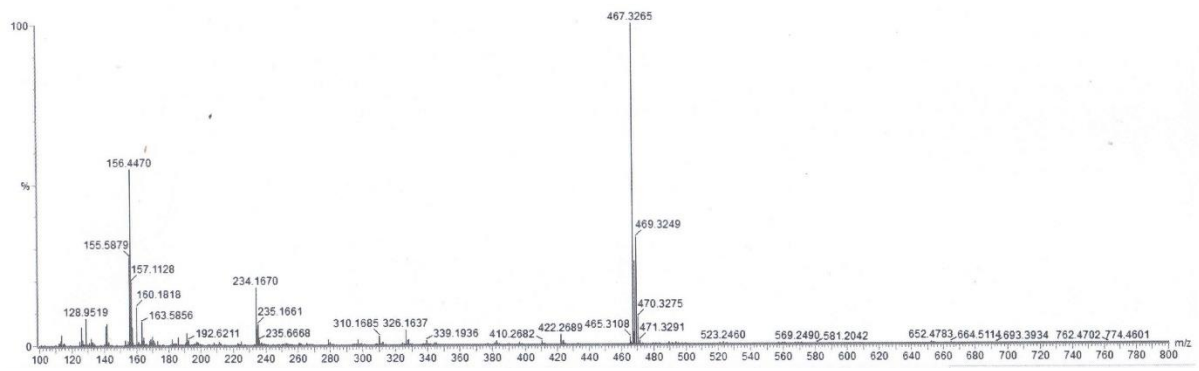


Fig. S3. Electrospray ionization mass spectrum (ESI-MS positive) of the Schiff base ligand in methanol (top) and its expanded view at bottom.

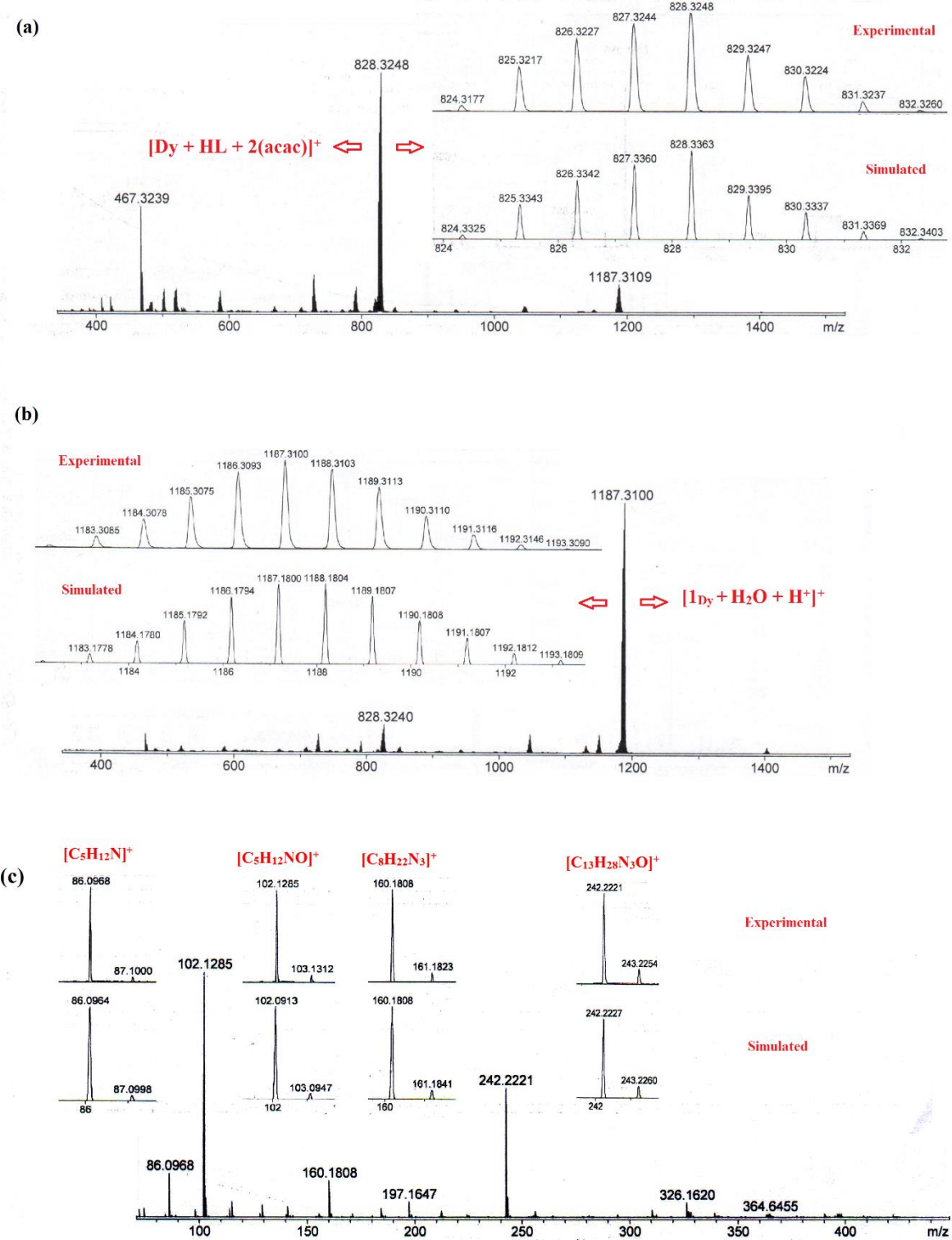
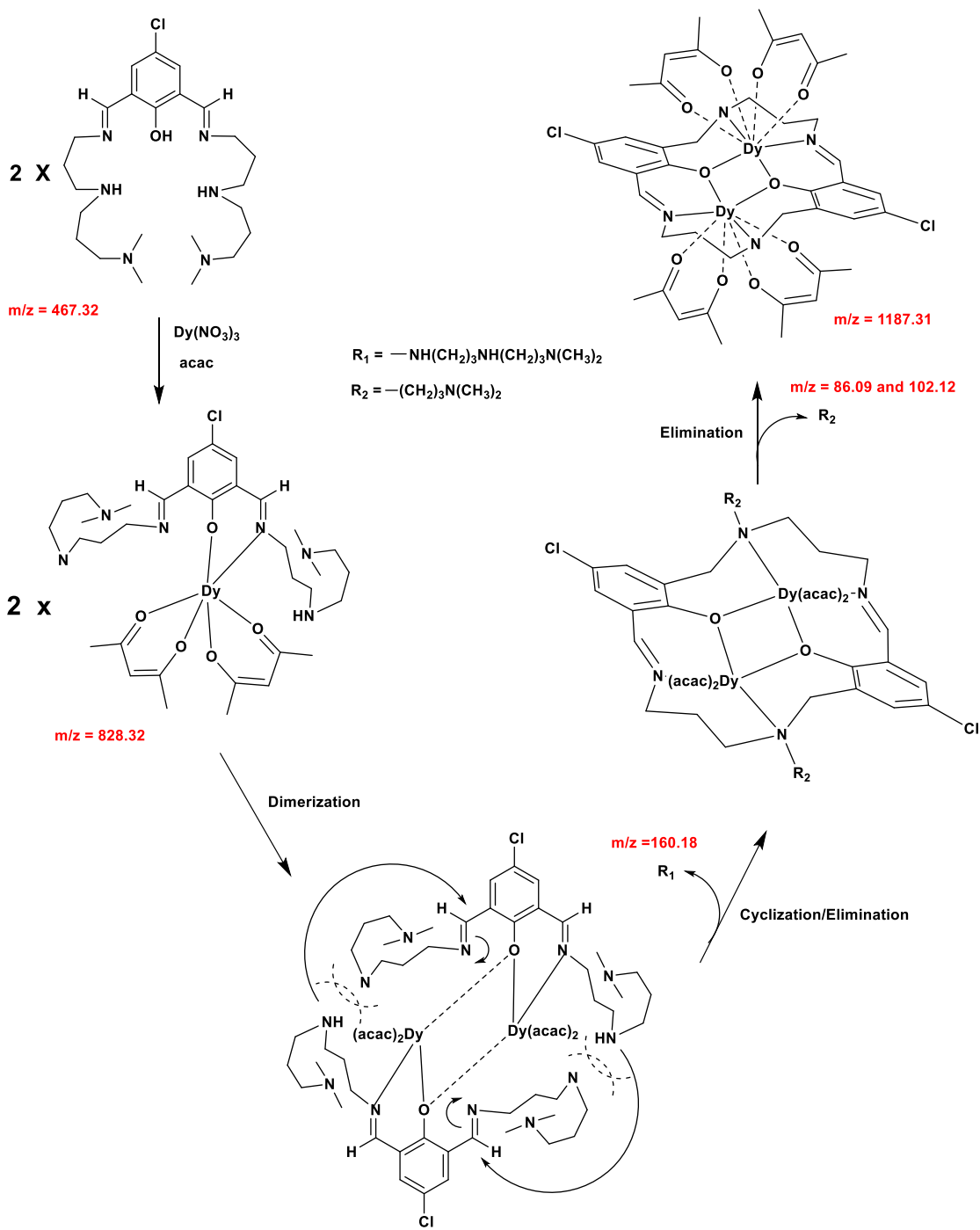


Fig. S4. Electrospray ionization mass spectra (ESI-MS positive) of a reaction mixture recorded after 5 min (top) and 1 h (bottom) of mixing.



Scheme S1. Probable mechanism for the *in-situ* transformation of the Schiff base leading to the macrocyclic ligand.

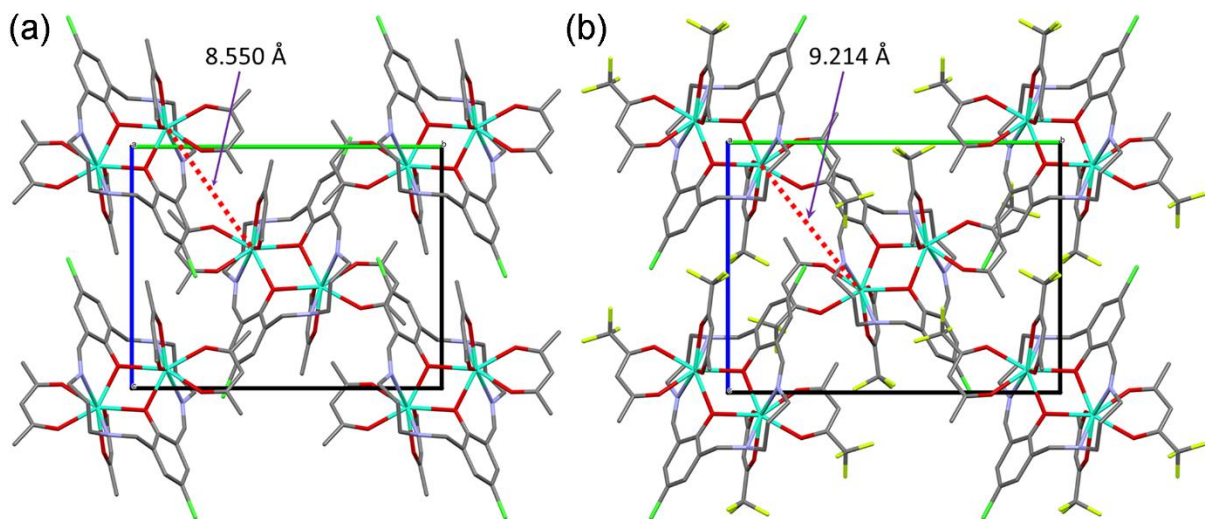


Fig. S5. Crystal packing of complexes **1_{Dy}** and **4_{Dy}** along the a axis. The numbers show the shortest Dy-Dy distances between the adjacent Dy_2 units.

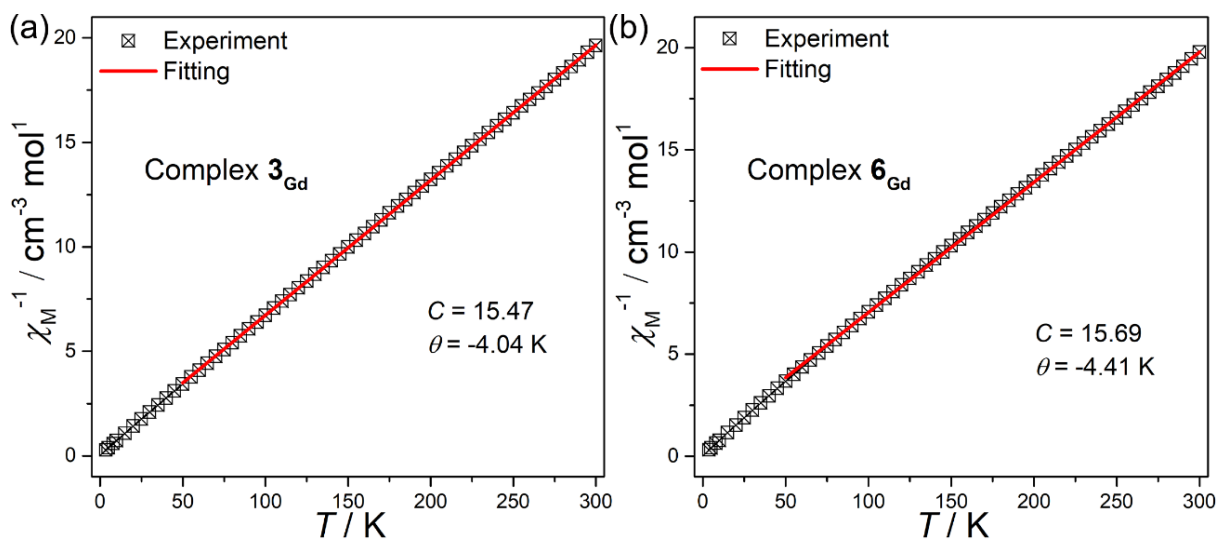


Fig. S6. The plot of $1/\chi_M$ versus T for **3_{Gd}** (a) and **6_{Gd}** (b), and the linear fit of Curie-Weiss law. The solid lines represent the best fits according to the Curie-Weiss law.

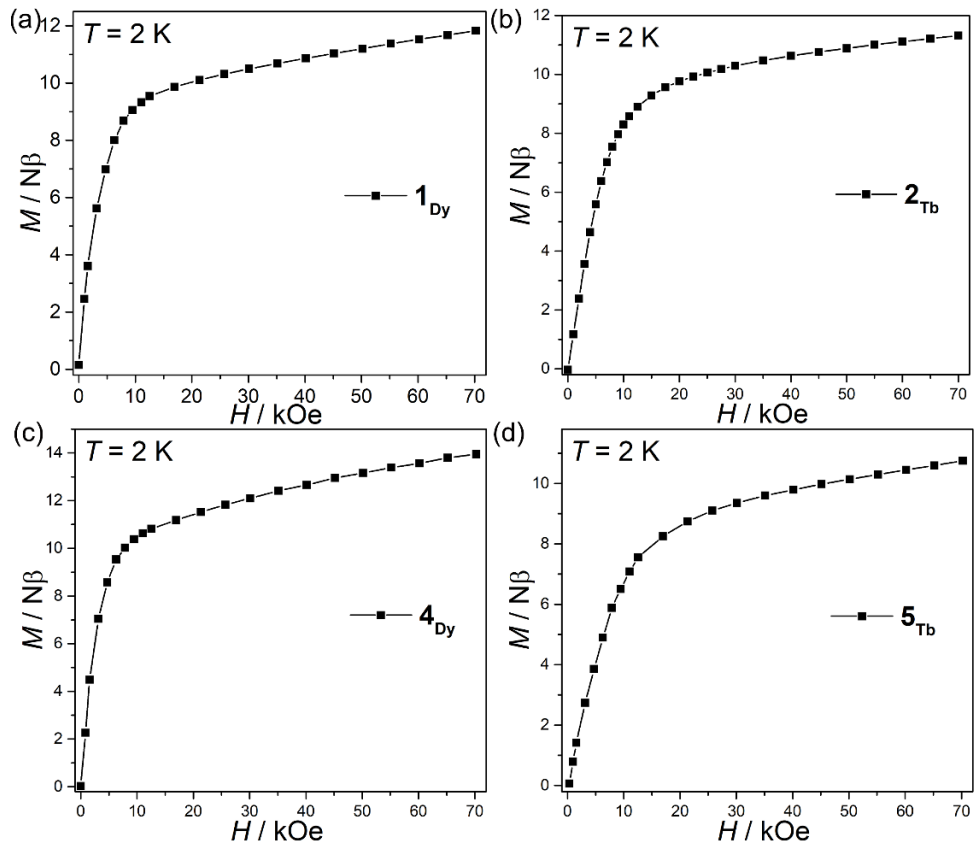


Fig. S7. Field dependent magnetization curves for compounds **1_{Dy}**, **2_{Tb}**, **4_{Dy}** and **5_{Tb}** at 2.0 K.

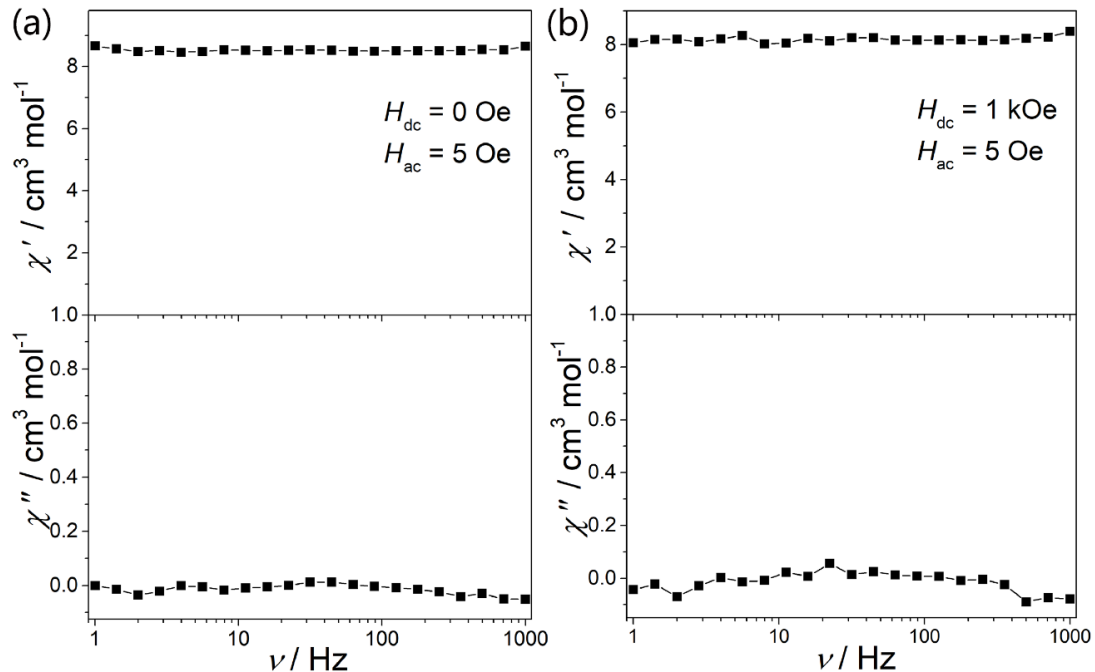


Fig. S8. Frequency dependent in-phase (χ') and out-of phase (χ'') signals of the ac susceptibility for **2_{Tb}** under applied $H_{dc} = 0$ and 1 kOe.

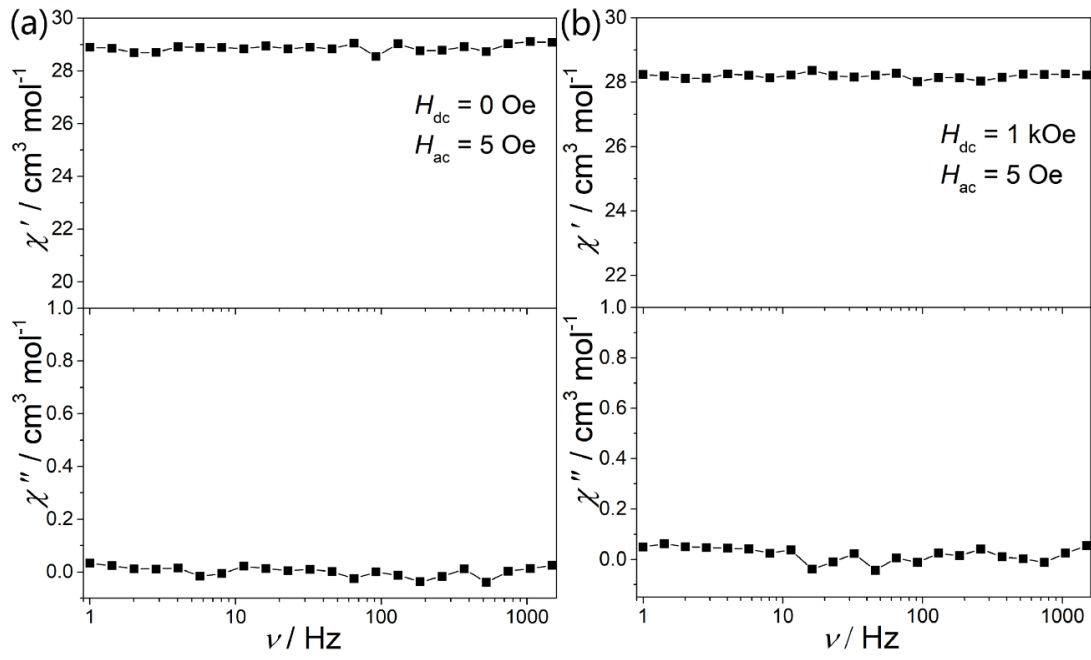


Fig. S9. Frequency dependent in-phase (χ') and out-of phase (χ'') signals of the ac susceptibility for **5Tb** under applied $H_{\text{dc}} = 0$ and 1 kOe.

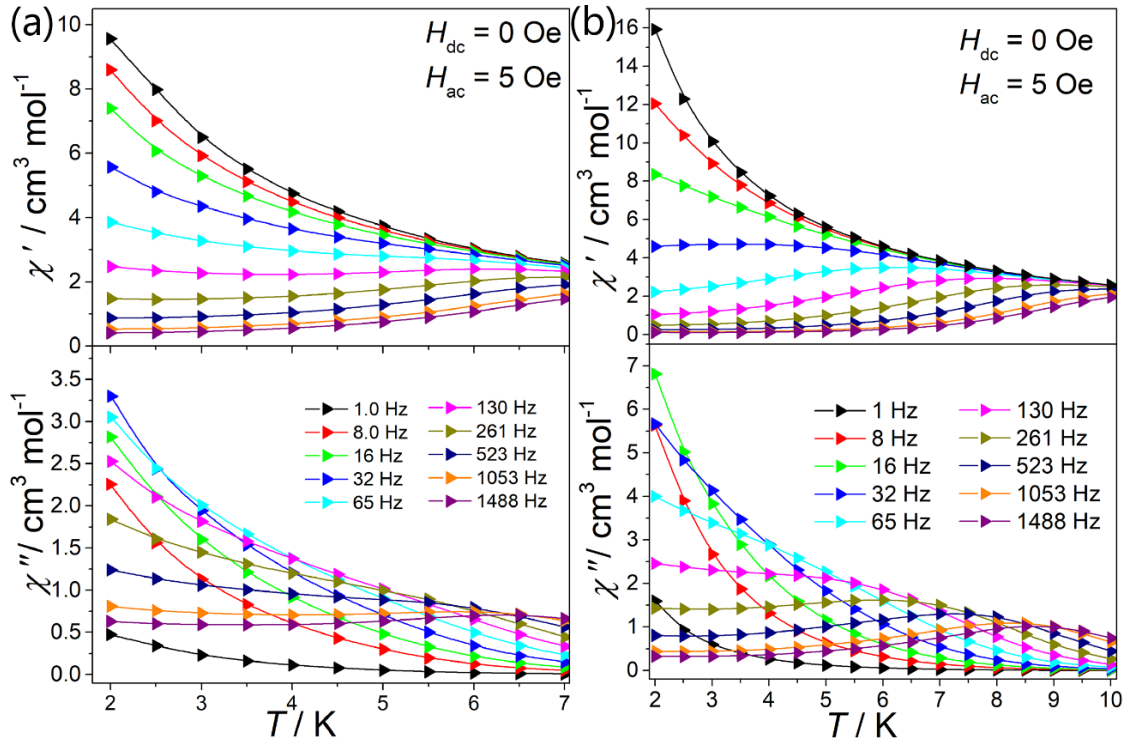


Fig. S10. Temperature dependent in-phase (χ') and out-of phase (χ'') signals of the ac susceptibility for **1Dy** and **4Dy** under zero dc field.

Electrostatic model for **1Dy** and **4Dy**

Electrostatic calculations. The electrostatic calculations were performed on the complete monometallic structures using the X-Ray geometry with no optimization. The charge on the ligands is expected to have a dominant role in the determination of the electrostatic potential experienced by Dy^{III}, and thus, the electrostatic field produced by charge on the ligands could be calculated within a minimal valence bond model. Within this model, the charge is delocalized as a resonance hybrid that can be seen as a weighted sum of all “chemically stable” Lewis structures. The electrostatic calculations were implemented in a MAGELLAN program. This model does not take account different electron withdrawing or donating groups in the charged ligands. The partial charges assigned to the formally charged ligands in complexes **1Dy** and **4Dy** were shown in Fig. S11.

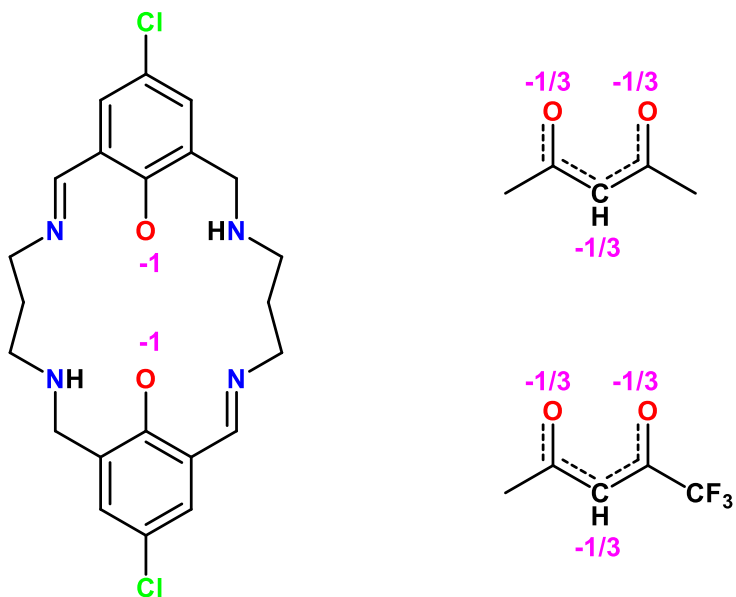


Fig. S11. Partial charges assigned to the formally charged ligands in complexes **1Dy** and **4Dy**.

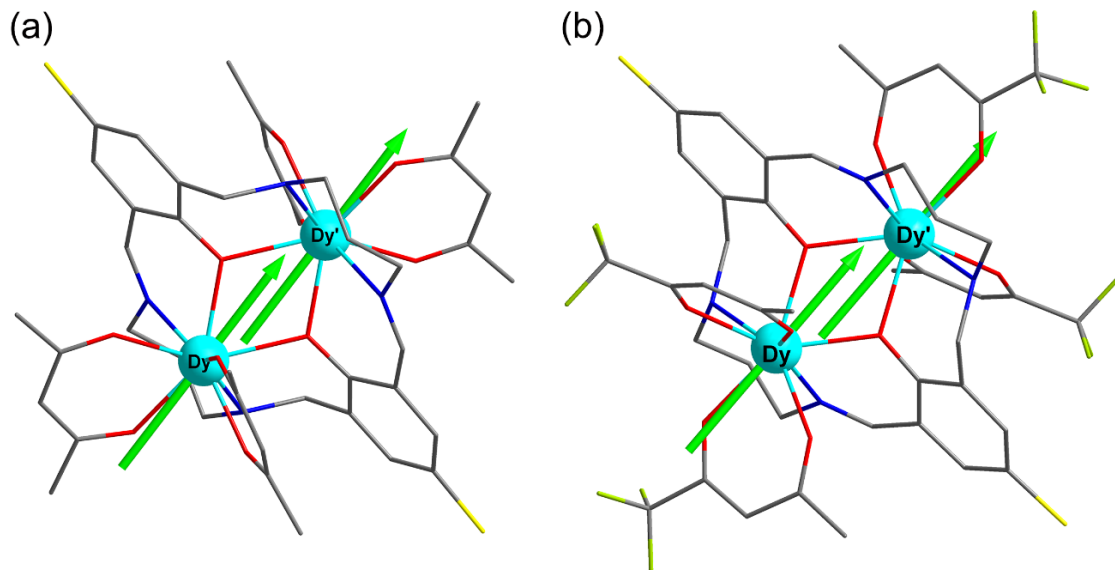


Fig. S12. Ground state magnetic anisotropy of complexes **1Dy** (a) and **4Dy** (b). The Green rods represent the orientations of the electrostatic anisotropy axes for each of the two Dy^{III} ions in complexes **1Dy** and **4Dy** as calculated by electrostatic model.

Table S1. Selected bond lengths (\AA) for complex **1Dy–6Gd**.

	1Dy	2Tb	3Gd	4Dy	5Tb	6Gd
Ln–O1	2.302(2)	2.306(2)	2.327(2)	2.2990(19)	2.307(2)	2.328(2)
Ln–O1'	2.371(2)	2.378(3)	2.405(2)	2.3402(19)	2.353(2)	2.381(2)
Ln–O2	2.321(2)	2.309(2)	2.357(2)	2.335(2)	2.349(2)	2.377(2)
Ln–O3	2.302(2)	2.330(2)	2.330(3)	2.324(2)	2.334(2)	2.358(2)
Ln–O4	2.323(2)	2.320(3)	2.345(3)	2.341(2)	2.349(3)	2.374(2)
Ln–O5	2.337(2)	2.338(3)	2.354(3)	2.364(2)	2.372(3)	2.393(2)
Ln–N1	2.595(2)	2.601(3)	2.624(3)	2.573(2)	2.592(3)	2.608(2)
Ln–N2	2.588(2)	2.593(3)	2.611(3)	2.564(2)	2.572(3)	2.595(2)
Ln…Ln'	3.891(1)	3.901(2)	3.939(1)	3.874(1)	3.895(1)	3.935(1)

Table S2. SHAPE analysis of the Ln^{III} ion in complexes **1Dy**–**6Gd**.

Label	Shape	Symmetry	1Dy	2Tb	3Gd	4Dy	5Tb	6Gd
OP-8	Octagon	<i>D</i> _{8h}	29.655	29.746	29.967	29.614	29.667	29.812
HPY-8	Heptagonal pyramid	<i>C</i> _{7v}	23.089	22.981	22.916	23.103	23.084	22.967
HBPY-8	Hexagonal bipyramid	<i>D</i> _{6h}	15.228	15.228	15.136	15.982	15.928	15.768
CU-8	Cube	<i>O</i> _h	9.516	9.474	9.373	9.645	9.562	9.415
SAPR-8	Square antiprism	<i>D</i> _{4d}	0.711	0.715	0.738	0.719	0.732	0.759
TDD-8	Triangular dodecahedron	<i>D</i> _{2d}	1.928	1.927	1.908	2.262	2.222	2.173
JGBF-8	Johnson gyrobifastigium J26	<i>D</i> _{2d}	14.799	14.738	14.685	15.450	15.464	15.376
JETBPY-8	Johnson elongated triangular bipyramid J14	<i>C</i> _{3h}	26.661	26.599	26.499	26.851	26.789	26.805
JBTPR-8	Biaugmented trigonal prism J50	<i>C</i> _{2v}	2.858	2.850	2.889	2.686	2.706	2.687
BTPR-8	Biaugmented trigonal prism	<i>C</i> _{2v}	2.403	2.394	2.411	2.209	2.194	2.158
JSD-8	Snub diphenoïd J84	<i>D</i> _{2d}	4.960	4.986	5.014	5.026	5.091	5.073
TT-8	Triakis tetrahedron	<i>T</i> _d	10.226	10.185	10.080	10.484	10.400	10.266
ETBPY-8	Elongated trigonal bipyramid	<i>D</i> _{3h}	22.882	22.798	22.704	22.496	22.423	22.359

Table S3. Relaxation fitting parameters from the least-square fitting of the Cole-Cole plots of **1Dy** under 2.0 K–7.0 K according to the generalized Debye model.

<i>T</i> / K	χ_s / cm ³ mol ⁻¹ K	χ_T / cm ³ mol ⁻¹ K	τ / s	α	<i>R</i>
2.0	0.09772	10.3948	0.00421	0.27892	0.10645
2.5	0.11156	8.22078	0.00338	0.2899	0.09519
3.0	0.14739	6.72181	0.00265	0.29167	0.07716
3.5	0.17321	5.68125	0.0021	0.29922	0.06261
4.0	0.20167	4.88581	0.00162	0.30654	0.04711
4.5	0.23683	4.26460	0.0012	0.31286	0.0359
5.0	0.27400	3.78384	8.44849E-4	0.31827	0.0291
5.5	0.30472	3.3875	5.49351E-4	0.31964	0.01956
6.0	0.32661	3.07392	3.37829E-4	0.32397	0.01335
6.5	0.32983	2.80968	1.93784E-4	0.33039	0.00906
7.0	0.29719	2.59099	1.07626E-4	0.34125	0.00549

Table S4. Relaxation fitting parameters from the least-square fitting of the Cole-Cole plots of **4Dy** under 2.0 K-10.0 K according to the generalized Debye model.

T / K	$\chi_s / \text{cm}^3 \text{mol}^{-1} \text{K}$	$\chi_T / \text{cm}^3 \text{mol}^{-1} \text{K}$	τ / s	α	R
2.0	6.86965E-4	16.1494	0.00931	0.12744	0.32776
2.5	0.08033	12.5575	0.00705	0.11972	0.30968
3.0	0.06263	10.2857	0.00549	0.12471	0.10584
3.5	0.05662	8.59557	0.00426	0.12479	0.07755
4.0	0.05857	7.34936	0.0033	0.12304	0.06592
4.5	0.05897	6.38985	0.00253	0.12444	0.05484
5.0	0.06854	5.66259	0.00193	0.12219	0.04426
5.5	0.07805	5.10091	0.00149	0.12397	0.0393
6.0	0.09391	4.62589	0.00114	0.12211	0.03583
6.5	0.11715	4.21506	8.46843E-4	0.1233	0.02997
7.0	0.1517	3.86827	6.21474E-4	0.125	0.02964
7.5	0.18891	3.57869	4.43622E-4	0.13162	0.02116
8.0	0.2364	3.32169	3.06309E-4	0.13671	0.01664
8.5	0.31043	3.0887	2.0806E-4	0.1361	0.01211
9.0	0.37057	2.89992	1.38155E-4	0.14039	0.00727
9.5	0.50749	2.73676	9.7337E-5	0.1303	0.00577
10.0	0.66957	2.58259	6.95075E-5	0.11459	0.00329

Table S5. Parameters fitted from the Arrhenius plots considering multiple relaxation processes for **1Dy** and **4Dy**.

Complex 1Dy			
	Value	Standard error	R^2
n	2.88	0.15	
C	8.19	1.91	
τ_{QTM}	0.0056	3×10^{-4}	0.9998
τ_0	$1.1 \times 10^{-8} \text{ s}$	3×10^{-9}	
U_{eff}	66.7 K	2.4	
Complex 4Dy			
	Value	Standard error	R^2
n	2.86	0.07	
C	4.40	0.53	
τ_{QTM}	0.013	6×10^{-4}	0.9998
τ_0	$3.3 \times 10^{-8} \text{ s}$	6×10^{-9}	
U_{eff}	79.0 K	1.8	

Computational details

Both of binuclear complexes **1Dy** and **4Dy** with central symmetrical structures have one type of magnetic center Dy^{III} ion. Complete-active-space self-consistent field (CASSCF) calculations on individual Dy^{III} fragments for **1Dy** and **4Dy** (see Figure S13 for the calculated complete structures of **1Dy** and **4Dy**) on the basis of single-crystal X-ray determined geometry have been carried out with MOLCAS 8.4^{S1} program package. Each individual Dy^{III} fragment in **1Dy** and **4Dy** was calculated keeping the experimentally determined structure of the corresponding compound while replacing the neighboring Dy^{III} ion by diamagnetic Lu^{III}.

The basis sets for all atoms are atomic natural orbitals from the MOLCAS ANO-RCC library: ANO-RCC-VTZP for Dy^{III}; VTZ for close N and O; VDZ for distant atoms. The calculations employed the second order Douglas-Kroll-Hess Hamiltonian, where scalar relativistic contractions were taken into account in the basis set and the spin-orbit couplings were handled separately in the restricted active space state interaction (RASSI-SO) procedure. Active electrons in 7 active spaces include all *f* electrons (CAS(9 in 7) in the CASSCF calculation. To exclude all the doubts, we calculated all the roots in the active space. We have mixed the maximum number of spin-free state which was possible with our hardware (all from 21 sextets, 128 from 224 quadruplets, 130 from 490 doublets for Dy^{II}. SINGLE_ANISO^{S2} program was used to obtain the energy levels, *g* tensors, magnetic axes, *et al.*, based on the above CASSCF/RASSI-SO calculations.

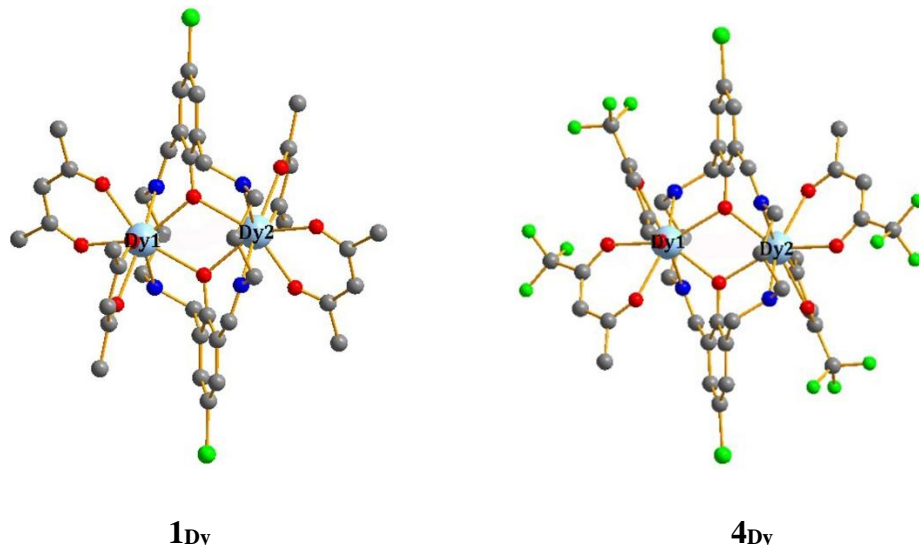


Fig. S13. Calculated complete structures of complexes **1Dy** and **4Dy**; H atoms are omitted.

Table S6. Calculated energy levels (cm^{-1}), \mathbf{g} (g_x , g_y , g_z) tensors and predominant m_J values of the lowest eight Kramers doublets (KDs) of individual Dy^{III} fragments for complexes **1_{Dy}** and **4_{Dy}** using CASSCF/RASSI-SO with MOLCAS 8.4.

KDs	1_{Dy}			4_{Dy}		
	E/cm^{-1}	\mathbf{g}	m_J	E/cm^{-1}	\mathbf{g}	m_J
1	0.0	0.017 0.034 19.159	$\pm 15/2$	0.0	0.005 0.009 19.498	$\pm 15/2$
2	96.9	0.245 0.305 15.736	$\pm 13/2$	143.1	0.146 0.240 15.964	$\pm 13/2$
3	175.1	0.177 0.604 12.802	$\pm 11/2$	224.4	0.561 0.785 13.214	$\pm 11/2$
4	231.5	2.316 2.776 9.962	$\pm 7/2$	304.5	0.946 2.062 10.678	$\pm 9/2$
5	272.0	8.496 6.080 3.486	$\pm 3/2$	378.2	0.122 3.616 7.278	$\pm 5/2$

6	313.3	1.500 2.107 14.679	$\pm 1/2$	430.3	9.628 7.452 3.313	$\pm 1/2$
7	355.0	0.358 1.043 18.087	$\pm 5/2$	490.1	0.520 1.273 18.407	$\pm 3/2$
8	491.4	0.004 0.008 19.753	$\pm 9/2$	591.0	0.015 0.020 19.775	$\pm 7/2$

Table S7. Wave functions with definite projection of the total moment $|m_J\rangle$ for the lowest two KDs of individual Dy^{III} fragments for complexes **1Dy** and **4Dy**.

	E/cm^{-1}	wave functions
1Dy	0.0	88.3% $ \pm 15/2\rangle$ +8.0% $ \pm 11/2\rangle$
	96.9	72.5% $ \pm 13/2\rangle$ +18.0% $ \pm 9/2\rangle$
4Dy	0.0	93.7% $ \pm 15/2\rangle$
	143.1	68.5% $ \pm 13/2\rangle$ +21.9% $ \pm 9/2\rangle$

To fit the exchange interactions in complexes **1Dy** and **4Dy**, we took two steps to obtain them. Firstly, we calculated individual Dy^{III} fragments using CASSCF/RASSI-SO to obtain the corresponding magnetic properties. Then, the exchange interactions between the magnetic centers were considered within the Lines model,^{S3} while the account of the dipole-dipole magnetic couplings were treated exactly. The Lines model is effective and has been successfully used widely in the research field of *d* and *f*-elements single-molecule magnets.^{S4}

For complexes **1Dy** and **4Dy**, there is only one type of \tilde{J}_1 .

The Ising exchange Hamiltonian is:

$$\hat{H}_{exch} = -\tilde{J} \overset{\wedge}{\tilde{S}}_{Dy1} \overset{\wedge}{\tilde{S}}_{Dy2} \quad (1)$$

The \tilde{J}_{total} is the parameter of the total magnetic interaction ($\tilde{J}_{total} = \tilde{J}_{dip} + \tilde{J}_{exch}$) between magnetic center ions. The $\tilde{S}_{Dy} = 1/2$ is the ground pseudospin on the Dy^{III} site. The dipolar magnetic coupling can be calculated exactly, while the exchange coupling constant was fitted through comparison of the computed and measured magnetic susceptibilities using the POLY_ANISO program.^{S2}

Table S8. Exchange energies E (cm⁻¹), the energy difference between each exchange doublets Δ_t (cm⁻¹) and the main values of the g_z for the lowest two exchange doublets of **1Dy** and **4Dy**.

	1Dy			4Dy		
	E	Δ_t	g_z	E	Δ_t	g_z
1Dy	0.00	0.72×10^{-5}	38.318	0.00	0.34×10^{-6}	38.997
4Dy	1.29	0.12×10^{-4}	0.000	1.86	0.62×10^{-6}	0.000

Reference

- S1 F. Aquilante, J. Autschbach, R. K. Carlson, L. F. Chibotaru, M. G. Delcey, L. De Vico, I. Fdez. Galván, N. Ferré, L. M. Frutos, L. Gagliardi, M. Garavelli, A. Giussani, C. E. Hoyer, G. Li Manni, H. Lischka, D. Ma, P. Å. Malmqvist, T. Müller, A. Nenov, M. Olivucci, T. B. Pedersen, D. Peng, F. Plasser, B. Pritchard, M. Reiher, I. Rivalta, I. Schapiro, J. Segarra-Martí, M. Stenrup, D. G. Truhlar, L. Ungur, A. Valentini, S. Vancoillie, V. Veryazov, V. P. Vysotskiy, O. Weingart, F. Zapata and R. Lindh, MOLCAS 8: New Capabilities for Multiconfigurational Quantum Chemical Calculations across the Periodic Table, *J. Comput. Chem.*, 2016, **37**, 506.
- S2 (a) L. F. Chibotaru, L. Ungur and A. Soncini, *Angew. Chem. Int. Ed.*, 2008, **47**, 4126; (b) L. Ungur, W. Van den Heuvel and L. F. Chibotaru, *New J. Chem.*, 2009, **33**, 1224; (c) L. F. Chibotaru, L. Ungur, C. Aronica, H. Elmoll, G. Pilet and D. Luneau, *J. Am. Chem. Soc.*, 2008, **130**, 12445.

- S3 M. E. Lines, *J. Chem. Phys.* 1971, **55**, 2977.
- S4 (a) K. C. Mondal, A. Sundt, Y. H. Lan, G. E. Kostakis, O. Waldmann, L. Ungur, L. F. Chibotaru, C. E. Anson and A. K. Powell, *Angew. Chem. Int. Ed.* 2012, **51**, 7550; (b) S. K. Langley, D. P. Wielechowski, V. Vieru, N. F. Chilton, B. Moubaraki, B. F. Abrahams, L. F. Chibotaru and K. S. Murray, *Angew. Chem. Int. Ed.* 2013, **52**, 12014.